Monthly Notices
of the
ROYAL ASTRONOMICAL SOCIETY

MNRAS **440,** 3091–3099 (2014) doi:10.1093/mnras/stu534

Disentangling the physical reality of star cluster candidates projected towards the inner disc of the Large Magellanic Cloud

Andrés E. Piatti[1,2]★

[1] *Observatorio Astronómico, Universidad Nacional de Córdoba, Laprida 854, 5000, Córdoba, Argentina*
[2] *Consejo Nacional de Investigaciones Científicas y Técnicas, Av. Rivadavia 1917, C1033AAJ, Buenos Aires, Argentina*

Accepted 2014 March 14. Received 2014 March 13; in original form 2014 March 3

ABSTRACT

We have used Washington photometry for 90 star cluster candidates of small angular size – typically ∼11 arcsec in radius – distributed within nine selected regions in the inner disc of the Large Magellanic Cloud (LMC) to disentangle whether they are genuine physical system, and to estimate the ages for the confirmed clusters. In order to avoid a misleading interpretation of the cluster colour–magnitude diagrams (CMDs), we applied a subtraction procedure to statistically clean them from field star contamination. Out of the 90 candidate clusters studied, 61 resulted to be genuine physical systems, whereas the remaining ones were classified as possible non-clusters since either their CMDs and/or the distribution of stars in the respective fields do not resemble those of stellar aggregates. We statistically show that $\sim(13 \pm 6)$ per cent of the catalogued clusters in the inner disc could be possible non-clusters, independently of their deprojected distances. We derived the ages for the confirmed clusters from the fit of theoretical isochrones to the cleaned cluster CMDs. The derived ages resulted to be in the age range $7.8 \leq \log(t) \leq 9.2$. Finally, we built cluster frequencies (CFs) for the different studied regions and found that there exists some spatial variation of the LMC CF throughout the inner disc. Particularly, the innermost field contains a handful of clusters older than ∼2 Gyr, while the wider spread between different CFs has taken place during the most recent 50 Myr of the galaxy lifetime.

Key words: techniques: photometric – galaxies: individual: LMC – Magellanic Clouds.

1 INTRODUCTION

Star clusters have long been key objects to reconstruct the formation and the dynamical and chemical evolutions of galaxies. As the Large Magellanic Cloud (LMC) is considered, the study of its star cluster population has allowed us to learn about its spread in metallicity at the very early epoch (Brocato et al. 1996); the existence of a relatively important gap in its age distribution (Geisler et al. 1997); the evidence of vigorous star cluster formation episodes (Piatti 2011b); the complexity of the cluster formation rate during the last million years (de Grijs, Goodwin & Anders 2013), etc. Although somewhat inhomogeneous and clearly still incomplete, the astrophysical properties estimated for a significant number of LMC star clusters have been the starting point to address galactic global issues such as the age–metallicity relationship and the cluster formation rate, among others. Therefore, it is of great importance to enlarge the number of objects confirmed as genuine star clusters and to estimate their fundamental parameters.

With the aim of providing mainly with age and metallicity estimates for an increasing number of LMC star clusters, we have continued a long-term observational programme carried out at Cerro Tololo Interamerican Observatory (CTIO) using different telescopes in conjunction with CCD cameras and the Washington photometric filters (Canterna 1976). A total of 61 clusters have been observed and their fundamental parameters estimated (see, e.g., Geisler et al. 1997, 2003; Piatti et al. 1999, 2002, 2003a,b, 2009, 2011). More recently, we took advantage of a wealth of available images at the National Optical Astronomy Observatory (NOAO) Science Data Management Archives,[1] obtained at the CTIO 4-m Blanco telescope with the Mosaic II camera attached (36×36 arcmin^2 field with a 8k × 8k CCD detector array, scale 0.274 arcsec pixel^{-1}) and the Washington filters. From the whole volume of observed LMC fields (see Piatti, Geisler & Mateluna 2012), we identified 206 clusters previously catalogued by Bica et al. (2008, hereafter B08) and studied 107 of them with some detail (Piatti 2011b, 2012b). In this work, we end up the series of studies of unknown or poorly known

★ E-mail: andres@oac.uncor.edu

[1] http://www.noao.edu/sdm/archives.php

LMC clusters with available Washington photometry by analysing the remaining objects in the aforementioned sample.

The paper is organized as follows: Washington C, T_1 data are presented in Section 2. The star cluster sample is described in Section 3, while the cleaning of the colour–magnitude diagrams (CMDs) and the estimation of the cluster ages are presented in Sections 4 and 5, respectively. We discuss the results and build cluster frequencies (CFs) in Section 6. Finally, conclusions of this analysis are given in Section 7.

2 DATA HANDLING

The Washington C, T_1 photometric data set used in this work were obtained from a comprehensive process that involved the reduction of the raw images, the determination of the instrumental photometric magnitudes, and the standardization of the photometry. We have already described in detail such steps not only in the works cited above, but also in Piatti (2011a,c, 2012a); Piatti & Bica (2012) and Maia, Piatti & Santos (2014). For this reason, we summarize here some specific issues in order to provide the reader with an overview of the photometry quality.

The data come from observations carried out on the nights of 2008 Dec. 18–20 through the CTIO 2008B-0192 programme (PI: D. Geisler). The nights resulted to be of excellent photometric quality – with a typical seeing of ∼1 arcsec (see table 1 of Piatti et al. 2012) – as judged by the rms errors from the transformation to the standard system (∼0.02 mag in each filter). From extensive artificial star tests, we showed that the 50 per cent completeness level is located at $C \sim 23.5$–24.5 mag and $T_1 \sim 23.0$–24.0 mag, depending on the crowding and exposure time (see Piatti et al. 2012). The photometric errors in the T_1 magnitude increase typically from $\sigma(T_1) \leq 0.01$ mag for the T_1 range ∼16.0–20.0 mag up to $\sigma(T_1) \sim 0.20$ mag for $T_1 = 24.0$ mag. The errors for the $C - T_1$ magnitudes resulted in $\sigma(C - T_1) \leq 0.01$ for the T_1 range ∼16.0–19.0 mag and increases exponentially up to $\sigma(T_1) \sim 0.30$ mag for $T_1 = 24.0$ mag. We here analyse cluster CMDs down to $T_1 \sim 22.0$ mag, which corresponds to a completeness level nearly 100 per cent and photometric errors $\sigma(T_1) \leq 0.05$ mag. Thus, our photometry yields accurate morphology and position of the main features in the observed CMDs of the studied fields.

3 DEFINING THE CLUSTER SAMPLE

Fig. 1 shows a schematic chart with the distribution of the cluster candidates catalogued by B08 (dots) and the positions of the Mosaic II fields wherein the objects studied here are located (boxes). Some of the clusters placed within these Mosaic II fields have been previously studied by different authors (Piatti 2011b, 2012b; Baumgardt et al. 2013; Choudhury, Subramaniam & Piatti 2014), while others have been discarded from this analysis since their photometric data are not complete due to the presence of saturated stars in their images (BSDL 351, 349, 1980, H88-267, 308, KMHK 1274, HS 81, OGLE 308, and SL 360). The final cluster candidate sample studied here contains 90 objects.

According to B08's catalogue, the objects under study are of small angular dimension, typically with radius between ∼8 and 19 arcsec with an average of 11 arcsec. Considering the LMC regions traced by Harris & Zaritsky (2009), some clusters appear projected towards the densest 30 Doradus, the Bar, and the outer Bar regions, while others are distributed within the North-west Void and the North-west Arm, which are less crowded. All these substructures are within the so-called inner LMC disc ($R < 4$ kpc; Bica et al. 1998). In addition,

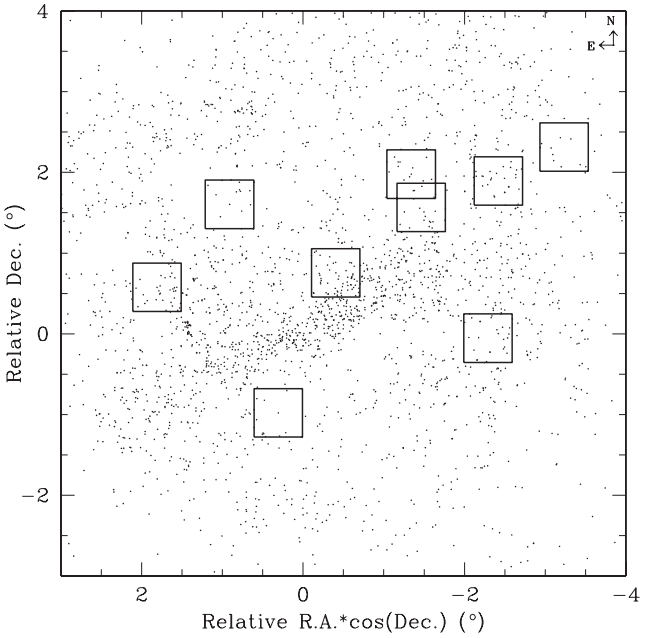

Figure 1. Distribution of the LMC star cluster candidates catalogued by Bica et al. (2008, dots) and the Mosaic II fields (boxes) wherein the studied objects are located.

many of the tiny selected objects are apparently composed by a handful of stars, which makes them of very low contrast over the background stellar density.

The clusters included in this study were first recognized by overplotting the positions of those catalogued by B08 to the deepest Mosaic II C, T_1 images, thus, avoiding to mismatch the observed objects and the actual list of catalogued clusters. We thus assigned to the observed clusters the respective names taken from B08. We searched for the same names in the Digital Sky Survey (DSS)[2] and downloaded 15 arcmin × 15 arcmin B images centred on the coordinates matched by the DSS. We used the SIMBAD astronomical data base as an additional source for checking the cluster coordinates. When comparing the DSS-extracted regions with the observed cluster fields in the C, T_1 images, we could confirm the positions of our selected targets. Note that, since most of the observed objects are of small angular size and many of them are projected towards relatively crowded fields with stellar density fluctuations, the task of distinguishing a star cluster from a chance grouping of stars was not at all straightforward. Table 1 contains a complete list of the recognized objects.

4 ANALYSIS OF THE CMDs

In general terms, the observed CMDs of the selected objects are the result of the superposition of different stellar populations distributed along the line of sight. For this reason, the use of the

[2] The Digitized Sky Surveys were produced at the Space Telescope Science Institute under U.S. Government grant NAG W-2166. The images of these surveys are based on photographic data obtained using the Oschin Schmidt Telescope on Palomar Mountain and the UK Schmidt Telescope. The plates were processed into the present compressed digital form with the permission of these institutions.

Table 1. Published and present LMC cluster fundamental parameters.

ID	RA (^{h} ^{m} ^{s})	Dec. ($^{\circ}$ $'$ $''$)	l ($^{\circ}$)	b ($^{\circ}$)	r (arcsec)	$E(B-V)$ (mag)	log(t/yr)	Note
GKK-O222	05 09 00	−67 59 00	278.704	−34.537	0.14	0.055	9.20	
HS 228	05 19 24	−68 52 52	279.522	−33.415	0.27	0.060	9.10	8.610 ± 0.055 (4)
H88-270	05 18 47	−69 16 37	279.999	−33.392	0.18	0.090	9.10	7.950 ± 0.150 (4)
HS 156	05 11 11	−67 37 37	278.227	−34.414	0.18	0.061	9.00	9.04 ± 0.04 (1)
SL 390	05 19 54	−68 57 53	279.609	−33.354	0.32	0.081	9.00	9.200 ± 0.030 (4)
BSDL 1334	05 21 14	−68 47 00	279.369	−33.271	0.18	0.060	9.00	
H88-259	05 17 20	−69 09 25	279.890	−33.542	0.18	0.081	8.90	
H88-276	05 19 55	−68 48 07	279.418	−33.384	0.23	0.060	8.90	8.180 ± 0.215 (4)
GKK-O220	05 10 18	−67 51 00	278.512	−34.447	0.23	0.060	8.90	
OGLE 264	05 15 21	−69 06 27	279.875	−33.725	0.18	0.078	8.80	
SL 124e	04 56 31	−69 58 54	281.410	−35.091	0.14	0.115	8.70	8.730 ± 0.170 (4)
SL 124w	04 56 29	−69 59 00	281.413	−35.094	0.14	0.115	8.70	
H88-261	05 17 26	−69 06 55	279.838	−33.542	0.32	0.081	8.70	
HS 200	05 15 36	−69 08 21	279.907	−33.697	0.18	0.086	8.70	8.250 ± 0.800 (4)
OGLE 122	05 07 19	−68 20 55	279.179	−34.605	0.18	0.059	8.60	
H88-260	05 17 20	−69 12 49	279.956	−33.530	0.18	0.090	8.60	
OGLE 271	05 15 39	−68 54 31	279.635	−33.741	0.27	0.078	8.60	
H88-285	05 21 03	−69 05 51	279.741	−33.229	0.18	0.081	8.50	8.070 ± 0.025 (4)
H88-326	05 43 29	−69 09 44	279.484	−31.242	0.18	0.072	8.50	8.45 ± 0.3 (2)
H88-249	05 16 31	−69 10 58	279.939	−33.608	0.14	0.090	8.50	
H88-286	05 21 07	−69 08 09	279.787	−33.216	0.14	0.081	8.50	8.45 ± 0.5 (2)
H88-272	05 19 05	−68 52 14	279.515	−33.445	0.23	0.060	8.50	
H88-252	05 16 43	−69 12 13	279.958	−33.586	0.23	0.090	8.40	8.470 ± 0.255 (4)
H88-34	04 55 39	−67 49 19	278.900	−35.793	0.14	0.058	8.40	8.250 ± 0.110 (4)
H88-32	04 55 39	−67 43 34	278.788	−35.819	0.14	0.058	8.40	8.150 ± 0.155 (4)
BSDL 194	04 54 05	−69 45 30	281.227	−35.359	0.14	0.102	8.40	8.640 ± 0.135 (4)
H88-325	05 43 15	−69 02 03	279.337	−31.275	0.18	0.072	8.35	
HS 113	05 05 54	−68 14 15	279.085	−34.759	0.23	0.059	8.30	
H88-253	05 16 50	−69 03 35	279.786	−33.605	0.18	0.081	8.30	
H88-240	05 16 04	−69 06 09	279.853	−33.664	0.27	0.081	8.30	8.650 ± 0.050 (4)
OGLE 346	05 19 09	−69 15 36	279.972	−33.363	0.25	0.090	8.20	
H88-281	05 20 21	−69 14 48	279.932	−33.262	0.23	0.090	8.20	8.270 ± 0.215 (4)
BRHT 62a	05 00 05	−67 48 03	278.736	−35.397	0.32	0.062	8.20	8.9 ± 0.5 (2)
BSDL 1364	05 21 46	−68 43 53	279.298	−33.233	0.09	0.060	8.20	
H88-287	05 21 09	−69 07 02	279.763	−33.216	0.23	0.081	8.20	8.310 ± 0.085 (4)
SL 408A	05 21 05	−69 04 16	278.896	−34.889	0.23	0.055	8.15	7.7 ± 0.3 (2)
HS 198	05 15 26	−69 03 02	279.807	−33.730	0.14	0.078	8.15	8.2 (3)
H88-313	05 41 21	−69 03 46	279.391	−31.441	0.18	0.064	8.10	7.930 ± 0.085 (4)
H88-232	05 15 22	−69 02 32	279.798	−33.737	0.18	0.078	8.10	8.140 ± 0.095 (4)
H88-306	05 40 24	−69 15 10	279.623	−31.505	0.14	0.063	8.10	
H88-238	05 15 47	−69 14 39	280.027	−33.659	0.23	0.090	8.10	7.950 ± 0.050 (4)
KMHK 1029	05 31 57	−67 52 43	278.122	−32.435	0.27	0.058	8.00	7.920 ± 0.055 (4)
BSDL 192	04 54 05	−69 40.90	281.138	−35.382	0.18	0.102	8.00	8.3 ± 0.3 (2)
BSDL 320	04 57 08	−70 06 42	281.542	−35.002	0.14	0.115	8.00	8.300 ± 0.200 (4)
KMHK 335	04 56 51	−70 06 03	281.537	−35.029	0.09	0.115	8.00	8.390 ± 0.060 (4)
HS 205	05 16 32	−68 55 07	279.627	−33.660	0.27	0.081	8.00	
OGLE 363	05 20 04	−69 15 55	279.959	−33.282	0.18	0.090	8.00	
OGLE 127	05 07 32	−67 34 13	278.252	−34.766	0.23	0.061	8.00	
KMHK 993	05 30 34	−68 09 27	278.469	−32.526	0.18	0.062	8.00	
H88-321	05 42 08	−69 22 00	279.737	−31.341	0.18	0.063	7.90	7.570 ± 0.090 (4)
BRHT 60b	04 56 25	−67 56 21	279.014	−35.691	0.14	0.060	7.90	7.6 ± 0.5 (2)
OGLE 297	05 16 52	−69 04 13	279.798	−33.600	0.27	0.081	7.90	7.610 ± 0.235 (4)
BSDL 87	04 50 58	−67 36 35	278.808	−36.279	0.18	0.050	7.90	7.500 ± 0.075 (4)
BRHT 45b	04 56 52	−68 00 20	279.078	−35.632	0.14	0.060	7.90	7.6 ± 0.5 (2)
NGC 1764	04 56 28	−67 41 41	278.724	−35.753	0.23	0.058	7.90	7.8 ± 0.3 (2)
H88-315	05 41 38	−69 18 48	279.680	−31.391	0.18	0.063	7.90	7.4 ± 0.5 (2)
HS 41	04 51 30	−67 27 15	278.605	−36.276	0.18	0.048	7.80	7.9 ± 0.3 (2)
H88-329	05 43 43	−69 13 23	279.554	−31.216	0.18	0.072	7.80	7.210 ± 0.110 (4)
NGC 1885	05 15 07	−68 58 43	279.729	−33.772	0.32	0.081	7.80	8.300 ± 0.030 (4)
OGLE 340	05 18 47	−69 13 32	279.939	−33.402	0.36	0.090	7.60	
H88-327	05 43 38	−69 15 51	279.603	−31.219	0.27	0.074	7.50	

Note. (1) Palma et al. (2013); (2) Glatt et al. (2010); (3) Pietrzyński & Udalski (2000); (4) Popescu et al. (2012, P12).

observed CMDs without subtracting the luminosity function and the colour distribution of stars belonging to the field might lead to wrong interpretations. Moreover, since the catalogued clusters have been identified as small star concentrations on the basis of a stellar density fluctuation in the sky, their real physical nature require a subsequent confirmation. In most of the cases, we probably deal with the presence of a genuine star cluster, while in other cases, it might constitute a chance grouping of stars or the effect of a non-uniform distribution of the interstellar material in that surveyed region. In order to disentangle cluster stars from field stars, it is required to employ CMDs of adjacent fields to subtract the local LMC field luminosity function and colour distribution.

We built cluster CMDs from all the measured stars distributed within a circle of radius three times those of the clusters. For this purpose, we used the radii (r) listed in Table 1, which were obtained from visual inspection of the objects in the deepest C, T_1 images. They are large enough so as to reach the observed field star region. Note that our main aim consists in cleaning the cluster CMDs from the contamination of field stars within areas around the clusters' centres nine times larger than πr^2, so that we did not need to trace their radial profiles. Once the cluster areas were delineated, we traced four additional regions with areas equals to the cluster regions and placed more or less equidistant to the clusters' centres around the cluster circular areas. From each surrounding region, we built a CMD which shows the features of the local LMC star field towards that particular direction. We then apply a procedure that compares each one of the field CMDs to the cluster CMD and subtract from the latter a representative field CMD in terms of stellar density, luminosity function, and colour distribution. We refer the reader to Piatti & Bica (2012) for details concerning this decontamination method. Each resultant representative field CMD is built from scanning the individual one using cells that vary in size, thus, achieving a better field representation than counting the number of stars in boxes fixed in size. Then, the stars in the cluster CMD that fall within the defined cells and closest to the representative positions are eliminated.

The method allows that cells vary in magnitude and colour separately according to the free path between field stars in the CMD, so that they result bigger in CMD regions with a small number of stars, and vice versa. The free path is defined as $\Delta(\text{colour})^2 + \Delta(\text{magnitude})^2 = (\text{free path})^2$, where Δ(colour) and Δ(magnitude) are the distances from the considered star to the closest one in abscissa and ordinate in the field CMD. In practice, an initial rectangular cell with a dimension of (Δ(colour), Δ(magnitude) = (0.5, 1.0) is put on a single field star. Then, the method looks for the closest star in magnitude and colour (it will be placed at a corner of the rectangular cell), so that the resulting closest magnitude and colour will be used to define the free path of the considered star. The task is repeated for every star in the field CMD. Therefore, each field star has associated a different cell. These cells are then superimposed to the cluster CMD, and the stars closest to their centres are eliminated. In this sense, the cell sizes depend not only on the stellar density of that field (the denser a field the more stars in the field CMD), but also on the magnitude and colour distributions of those field stars in the CMD, making some parts of the field CMD more populated than others. For instance, relatively bright field red giants with small photometric errors usually appear relatively isolated at the top-right zone of the CMD, while faint main-sequence (MS) stars are more numerous at the bottom part of the CMD. For this reason, bigger cells are required to satisfactorily subtract stars from the cluster CMD regions where there is a small number of field stars, while smaller cells are necessary for those CMD regions more populated by field stars.

After repeating the procedure of subtracting stars from the cluster CMD using the four selected surrounding fields, we obtained four cleaned cluster CMDs which were compared to each other. As a general rule, each star keeps not subtracted a different number of times in the four cleaned CMDs; the more the times a star is subtracted, the higher the probability of being a field feature. Thus, we convert the number of times that a star appears in the four cleaned cluster CMDs in an estimation of its probability (P) of being a fiducial feature in that cluster CMD. For instance, stars that are considered to belong to the field population appear once, or do not appear in the four cleaned cluster CMDs (we refer to them as of $P \leq 25$ per cent); stars that could indistinguishably belong to the field or to the studied object are seen twice ($P = 50$ per cent); and stars that are pre-dominantly found in the cleaned cluster area rather than in the star field population ($P \geq 75$ per cent) are identified more than twice. Whenever the CMDs for stars with $P \leq 25$ per cent looks like that of $P \geq 75$ per cent, we conclude that both the star field and the cluster are of similar features (ages).

To illustrate the bulk of the analysis performed, we produced multiple panel figures for the objects listed in Table 1. As an example, we include Fig. 2, which depicts three CMDs and an enlargement of the T_1 image centred on SL 390. We overplotted to the enlarged image a circle representing the cluster radius used in the analysis and marked the stars that have a chance of being cluster members

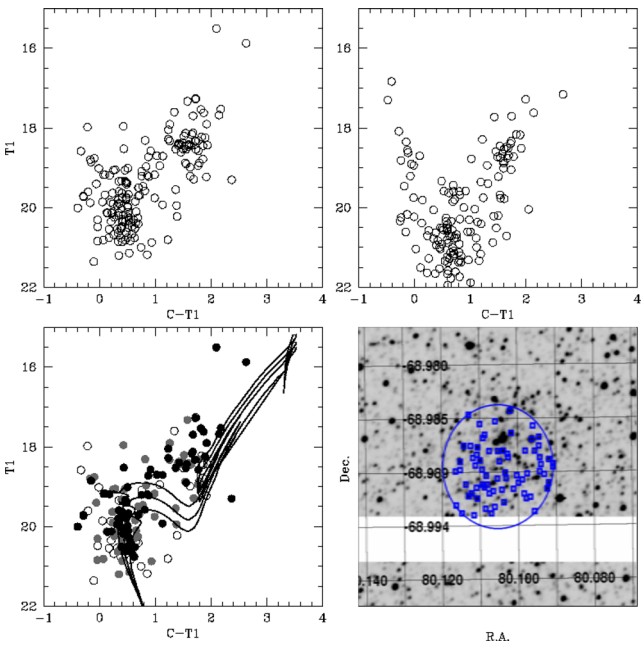

Figure 2. CMDs for stars in the field of SL 390: the observed CMD for the stars distributed within the cluster radius (upper-left panel); a field CMD for an annulus centred on the cluster, with an internal radius three times the cluster radius and an area equal cluster area (upper-right panel); the cleaned cluster CMD (bottom-left panel). Colour-scaled symbols represent stars that statistically belong to the field ($P \leq 25$ per cent, white), stars that might belong either to the field or to the cluster ($P = 50$ per cent, grey), and stars that pre-dominantly populate the cluster region ($P \geq 75$ per cent, black). Three isochrones from Marigo et al. (2008) for log(t) (see Table 1) and log(t) $\pm$ 0.10 are also superimposed. An enlargement of the T_1 image centred on the cluster with a circle representing the adopted cluster radius and stars with $P \geq 75$ per cent marked is shown in the bottom-right panel. North is upwards and east is to the left.

$P \geq 75$ per cent. The three CMDs represent the observed cluster CMD for the stars measured within the cluster radius (upper-left panel); a single field CMD for an annulus centred on the cluster, with an internal radius three times that of the cluster and an equal cluster area (upper-right panel); and the cleaned cluster CMD (bottom-left panel). The colour scale represents stars that statistically belong to the field ($P \leq 25$ per cent, white), stars that might belong either to the field or to the cluster ($P = 50$ per cent, grey), and stars that predominantly populate the cluster region ($P \geq 75$ per cent, black). The multiple panel figures for the entire sample of clusters can be found in the online version of the journal as Supplementary Information.

The distribution of stars with different membership probabilities in the CMD as well as in the cluster field were used at a time to confirm the physical reality of the studied cluster candidates. We required that the stars with $P \geq 75$ per cent within the cluster radius have as a counterpart a CMD resembling that of a star cluster to conclude that we are dealing with a genuine physical system. In some cases, we reinforced our conclusion about the nature of an object from the analysis of the distribution of stars with $P = 50$ and $\leq$25 per cent, respectively. We found that a handful of objects could be possible non-clusters, since either the CMDs and/or the distribution of stars in the respective fields do not resemble that of an stellar aggregate (BSDL 218, 256, 616, 661, 1103, 2794, 2824, 2841, 2842, 2891, 2898, BRHT 60a, 62b, GKK-O155, 203, 205, H88-248, 318, KMHK 125, 237, 258, 289, 609, 897, OGLE 291, 303, 335, 344, and SL 371). Fig. 3 depicts the results for BSDL 616, where the cleaned CMD shows an MS and a red clump (RC) mostly composed by field stars. Other possible non-clusters resulted to be

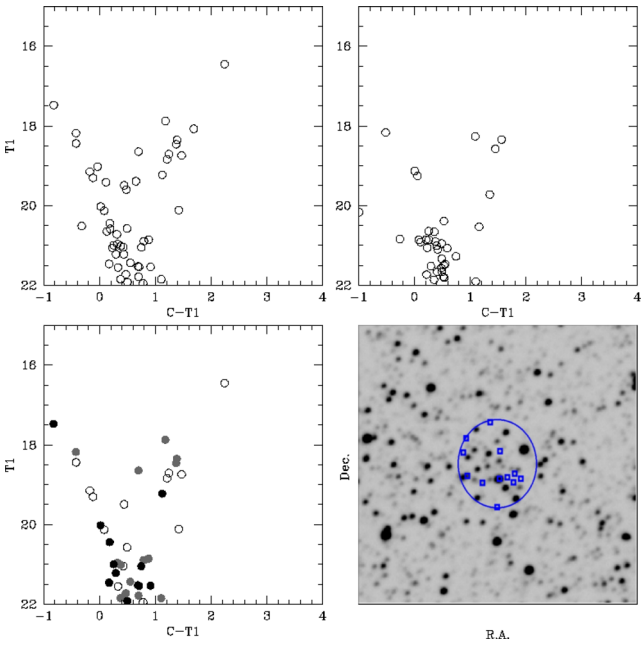

Figure 3. CMDs for stars in the field of BSDL 616: the observed CMD for the stars distributed within the cluster radius (upper-left panel); a field CMD for an annulus centred on the cluster, with an internal radius three times the cluster radius and an area equal cluster area (upper-right panel); the cleaned cluster CMD (bottom-left panel). Colour-scaled symbols represent stars that statistically belong to the field ($P \leq 25$ per cent, white), stars that might belong either to the field or to the cluster ($P = 50$ per cent, grey), and stars that pre-dominantly populate the cluster region ($P \geq 75$ per cent, black). An enlargement of the T_1 image centred on the cluster with a circle representing the adopted cluster radius and stars with $P \geq 75$ per cent marked is shown in the bottom-right panel. North is upwards and East is to the left.

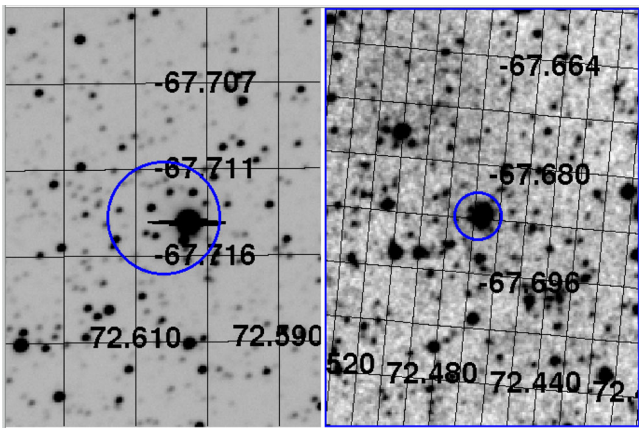

Figure 4. An enlargement of the T_1 image centred on KMHK 125 (left-hand panel) and that from the DSS image (right-hand panel). North is up and east is to the left. Note that the T_1 image is set on the telescope coordinates.

single bright stars surrounded by unresolved faint ones. Fortunately, the Mosaic II images have a better resolution and a fainter magnitude limit than those used for catalogued cluster candidates (see details in Piatti & Bica 2012), so apparent compact extended objects could be resolved. As an example, Fig. 4 compares an enlargement of the T_1 image centred on KMHK 125 to that obtained from the DSS.

5 CLUSTER AGE ESTIMATES

We estimated ages for the 61 confirmed star clusters by using the set of theoretical isochrones computed by Marigo et al. (2008) for the Washington photometric system. The isochrones were first reddened by the appropriate cluster colour excesses and corrected due to the distance effect. Then, we superimposed those for a metallicity level of $Z = 0.008$ to the cluster CMDs and chose the ones which best reproduced the cluster features to assign the cluster ages. The matching procedure was performed using stars with $P \geq 75$ per cent.

The estimation of cluster reddening values was made by interpolating the extinction maps of Burstein & Heiles (1982, hereafter BH). BH maps were obtained from H I (21 cm) emission data for the southern sky. They furnish us with foreground $E(B-V)$ colour excesses which depend on the Galactic coordinates. We also took advantages of the Magellanic Clouds extinction values based on RC stars photometry provided by the OGLE collaboration (Udalski 2003) as described in Haschke, Grebel & Duffau (2011). They resulted in average (0.02 ± 0.01) mag smaller than those obtained by BH. As for the Schlegel, Finkbeiner & Davis (1998) full-sky maps from 100-μm dust emission, we decided not to use them since the authors found that deviations are coherent in the sky and are especially conspicuous in regions of saturation of H I emission towards denser clouds and of formation of H_2 in molecular clouds. The relatively small angular sizes of the clusters did not allow us to trace reddening variations in any extinction map. Finally, we adopted the values obtained from the BH's maps, which are listed in Table 1. Their accuracy is 0.01 mag in $E(B-V)$ or 10 per cent of the reddening, whichever is larger. Note that a relative $C-T_1$ colour shift smaller than ∼0.05 mag hardly turns into a meaningful difference when matching isochrones of the same metallicity to the cluster MSs. Likewise, the mean $C-T_1$ colour difference for isochrones of the same age and with the closest metallicity

values that the Washington photometric system is able to distinguish (Δ([Fe/H]) = 0.20 dex; Geisler et al. 1997) results larger than ∼0.20 mag. Consequently, the reddening uncertainties do not affect either the age or the metallicity adopted for the clusters.

The LMC is located at a distance of 50 kpc (Subramanian & Subramaniam 2010) and according to Subramanian & Subramaniam (2009) it has an average depth of (3.44 ± 1.16) kpc, which implies a difference in its distance modulus as large as $\Delta((m - M)_o) \sim 0.30$ mag. Given that the clusters could be placed in from of, or behind the LMC, the simple assumption that all of them are at the same distance would lead to age uncertainties of $\sigma(\log(t)) \leq 0.06$. However, the age difference of the isochrones with the same metallicity bracketing the observed cluster MSs resulted to be in average $\Delta(\log(t)) = 0.20$. Therefore, we decided to adopt the value of the LMC distance modulus $(m - M)_o = 18.493 \pm 0.008$ reported by Pietrzyński et al. (2013) for all the clusters. Indeed, we generally found an excellent match.

As for the cluster metallicity, we adopted the same value for all of them. Piatti & Geisler (2013) showed that during the last 3 Gyr (the age range of our cluster sample) the LMC cluster population has chemically evolved or spread within the range [Fe/H] = (−0.4 ± 0.2) dex. On the other hand, according to the Washington photometry metallicity sensitivity, we should use isochrones for metallicity levels in steps of Δ([Fe/H]) = 0.20 dex. Further, higher metallicity resolution would lead to negligible changes in the isochrones overplotted on the cluster CMDs. However, we found that only isochrones with the same age and metallicity differences larger than Δ([Fe/H]) ∼ 0.30–0.40 dex can be meaningfully differentiated due to the dispersion of the stars. For this reason, we adopted a mean value of [Fe/H] = −0.40 dex for cluster metallicities, and assumed an error of σ([Fe/H]) = 0.20 dex.

In the matching procedure, which was performed looking at the cluster CMD, we used a subset of isochrones and superimposed them on the cluster CMDs, once they were properly shifted by the corresponding $E(C - T_1) = 1.97 \times E(B - V)$ colour excesses and by the LMC apparent distance modulus ($M_{T_1} = T_1 + 0.58E(B - V) - (V - M_V)$) (Geisler & Sarajedini 1999). Finally, we adopted as the cluster age the one corresponding to the isochrone which best reproduced the cluster main features in the CMD. The presence of RCs and/or red giant branch stars in some cluster CMDs made the matching procedure easier. Table 1 lists the resulting age estimates, while the bottom-left panel in Fig. 2 (likewise the online figures) shows the corresponding isochrones superimposed. The observed dispersion seen in the cluster CMDs can be encompassed with a couple of isochrones bracketing the derived mean age by $\Delta(\log(t)) = \pm 0.10$. We also included these adjacent isochrones in Fig. 2 (bottom-left panel).

37 clusters in the sample have previous age estimates (see Table 1). Palma et al. (2013) made use of Washington C, T_1 photometry obtained at the CTIO Blanco telescope and the MOSAIC II camera and derived an age of $\log(t) = 9.04 \pm 0.04$ for HS 156, in excellent agreement with our present value (9.00 ± 0.10). We also found a tight agreement with Pietrzyński & Udalski (2000), who derived from OGLE data an age of $\log(t) = 8.2$ for HS 198 (8.15 ± 0.10).

A more careful analysis requires the comparison of our ages with those of Glatt, Grebel & Koch (2010, hereafter G10) and Popescu, Hanson & Elmegreen (2012, hereafter P12) for 10 and 25 clusters in common, respectively. G10 used data from the Magellanic Clouds Photometric Survey (Zaritsky et al. 2002) of clusters mostly distributed in the main body of the galaxy, which is highly crowded. Although they mention that field contamination is a severe effect in the extracted cluster CMDs and therefore influences the age estimates, no decontamination from field CMDs was carried out. It would not be unexpected that some of the studied objects are not real star clusters, particularly those with very uncertain age estimates [$\sigma(\log(t)) \geq 0.5$]. Indeed, G10 estimated an age value for KMHK 125 of $\log(t) = 7.2 \pm 0.3$, for which our study suggests that it could be a possible non-cluster (see. Fig. 4). This possibility alerts us to the fact that solely the circular extraction of the observed CMDs of clusters located in highly populated star fields is not enough neither for an accurate isochrone fitting to the cluster MSs nor for confirming their physical nature. Zaritsky et al. (2002) found little visible evidence for incompleteness for $V < 20$ mag, corresponding to an MS turnoff of $\log(t) \approx 8.7$. The present CT_1 data set nearly reaches the 100 per cent completeness level at $T_1 \sim 22.0$ mag, which corresponds to MS turnoffs of $\log(t) \sim 9.6$. Furthermore, the scale of our images is 0.274 arcsec pixel^{-1}, while that of the Magellanic Cloud Photometric Survey is 0.7 arcsec pixel^{-1}, so that crowding effects at the centre of the objects is more important in their images.

P12 derived ages from integrated photometry for the clusters of Hunter et al. (2003). As is well known, the integrated light brings information about the composite stellar population distributed along the line of sight. For clusters of small angular size projected towards relatively crowded fields, the field contamination and stochastic effects, in addition to less deep photometric data could mislead the data analysis. Indeed, Baumgardt et al. (2013) compared the ages coming from Pietrzyński & Udalski (2000), G10, and P12 and then, due to the large uncertainties in ages coming from integrated magnitudes and colours, assigned ages to the clusters giving the highest priority to *Hubble Space Telescope* ages from Mackey & Gilmore (2003), followed by G10, the OGLE data, and finally P12. The best-fitting relation between G10 and P12 over 293 clusters in common resulted in a slope of 1.35 ± 0.35 and in a Pearson coefficient of 0.77. From this result, Baumgardt et al. (2013) concluded that there exists good agreement between G10 and P12.

Fig. 5 shows the comparison between the ages derived by G10 (left-hand panel) and P12 (right-hand panel) and our present values. The error bars correspond to the age uncertainties quoted by the authors, while the thick and thin lines represent the identity relationship and those shifted by $\pm 1\sigma(\log(t)_{\rm our})$, respectively. Black filled squares represent clusters that do not fulfil the requirement $\sigma(\log(t)_{\rm our}) + \sigma(\log(t)_{\rm pub}) \geq |\log(t)_{\rm our} - \log(t)_{\rm pub}|$. As can be seen,

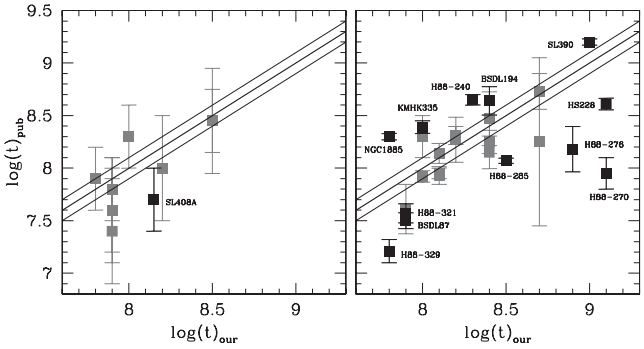

Figure 5. Difference between G10 (left-hand panel) and P12 (right-hand panel) and present age values. The error bars refer to age uncertainties quoted by the authors, and the thick and thin lines represent the identity relationship and those shifted by $\pm 1\sigma(\log(t)_{\rm our})$, respectively. Black filled squares represent clusters that do not fulfil the requirement $\sigma(\log(t)_{\rm our}) + \sigma(\log(t)_{\rm pub}) \geq |\log(t)_{\rm our} - \log(t)_{\rm pub}|$.

there is reasonable agreement, although several clusters significantly depart from the $\pm 1\sigma$ strip. We have carefully checked our multipanel Fig. 2 (online material) in order to seek a possible explanation for such deviations and found out that stochastic effects caused by the presence of isolated bright stars, a significant field contamination, and a less faint magnitude limit could be some of the factors that affected the integrated light, and hence the P12's age estimates. Particularly, the presence of a young field MS could cause the P12's age for H88-270 and HS 228 appear younger than our values. Conversely, an old field population could cause BSDL 194, H88-240, and SL 390 appear older at their integrated light. Examples of the presence of isolated bright stars can be BSDL 87, H88-238, 276, among others. We conclude that the present results point the need of a better study of the LMC clusters with, e.g., 8-m class telescopes.

6 DISCUSSION

Our results suggest that nearly 2/3 of the studied candidate star clusters would appear to be genuine physical systems. We also show that the ages derived by G10 and P12 can reflect those of the composite stellar populations of the LMC field. As far as we are aware, this is the first time that evidence is presented showing that some LMC candidate star clusters are not possible genuine physical systems.

In order to examine whether there exists any dependence of the fraction of possible non-clusters with the position in the LMC, we have made use of the central deprojected galactocentric distances of the nine Mosaic II fields computed by assuming that they are part of a disc having an inclination $i = 35\overset{\circ}{.}8$ and a position angle of the line of nodes of $\Theta = 145^{\circ}$ (Olsen & Salyk 2002). We refer the reader to table 1 of Subramanian & Subramaniam (2010) which includes a summary of orientation measurements of the LMC disc plane, as well as their analysis of the orientation and other LMC disc quantities, supporting the present adopted values. Note that most of the clusters catalogued by B08 located within the Mosaic fields have already been studied previously – we have made use of them here – (G10; Piatti & Geisler 2013) and in this work, so that there are no incompleteness effects in the estimated fraction of possible non-clusters in these areas.

Fig. 6 illustrates the behaviour of the proportion of possible non-clusters as a function of the deprojected distance. As can be seen, there exists no visible trend but an averaged fraction of 0.13 ± 0.06 within the LMC inner disc (distance from the LMC centre $\leq 4^{\circ}$; Bica et al. 1998). This does not seem to be a significant percentage of the catalogued clusters. If we assume a similar percentage for the whole catalogued LMC clusters distributed throughout the inner disc, we would expect that some, $\sim(300 \pm 140)$, objects were not real stellar aggregates. In the case that the possible non-clusters had their own spatial distribution, it would be possible to recover the expected spatial distribution of genuine star clusters by using the former to correct that of the catalogued clusters.

We finally built the CFs – the number of clusters per time unit as a function of age (Baumgardt et al. 2013) – for the nine studied LMC regions with the aim of investigating their variations in terms of the position in the galaxy recently reported by Piatti (2014, hereafter P14). Particularly, he found that 30 Doradus turns out to be the region with the highest relative frequency of the youngest clusters, while the $\log(t) = 9$–9.5 (1–3 Gyr) age range is characterized by cluster formation at a higher rate in the inner regions (e.g. Bar, outer Bar; see Harris & Zaritsky 2009) than in the outer ones (e.g. Blue Arm, Constellation III, South-east arm).

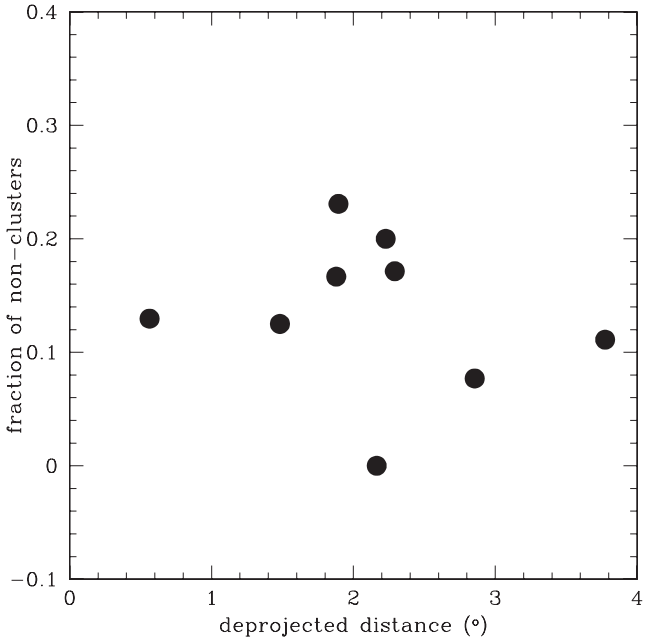

Figure 6. Fraction of possible non-clusters as a function of the deprojected distance (see text for details).

When building the CFs, we took into account the unavoidable complication that the cluster ages have associated uncertainties. Indeed, by considering such errors, the interpretation of the resulting CFs can differ appreciably from those obtained using only the measured ages without accounting for their errors. However, the treatment of age errors in the CF is not a straightforward task. This happens when an age value does not fall in the bin centre and, due to its errors, has the chance to fall outside it. Note that, since we chose bin dimensions as large as the involved errors, such points should not fall on average far beyond the adjacent bins. However, this does not necessarily happen for all the age values, and we should consider at the same time any other possibility. We followed the procedure outlined by P14, which achieves a compromise between the age bin size and the age errors. Particularly, we considered the possibility that the extension covered by an age value (properly a segment of $2 \times \sigma(\text{age})$ long) may have a dimension smaller, similar, or larger than the age bin wherein it is placed. The assigned weight was computed as the fraction of its age segment that falls in the age bin.

Fig. 7 shows the resultant CFs built from the catalogue of cluster ages compiled by P14 and from the ages estimated in this work, which encompass 90 per cent of the whole sample of catalogued clusters located in the studied LMC regions. The CFs have been normalized to the total number of clusters used. We have used the deprojected distances of Fig. 6 as the independent spatial variable. At first glance, we confirm the existence of spatial variations of the LMC CF throughout the inner disc. However, we do not rule out that some percentage of such a variation comes from the fact that we are dealing with relatively small areas and consequently some age regimes result not well sampled. Nevertheless, Fig. 7 suggests that the innermost field contains a handful of clusters older than $\sim$2 Gyr; the epoch of an important burst of cluster formation that took place after a cluster age gap (Piatti et al. 2002; Piatti 2011b). It also shows that there has been a wider spread between different CFs during the most recent 50 Myr of the galaxy lifetime.

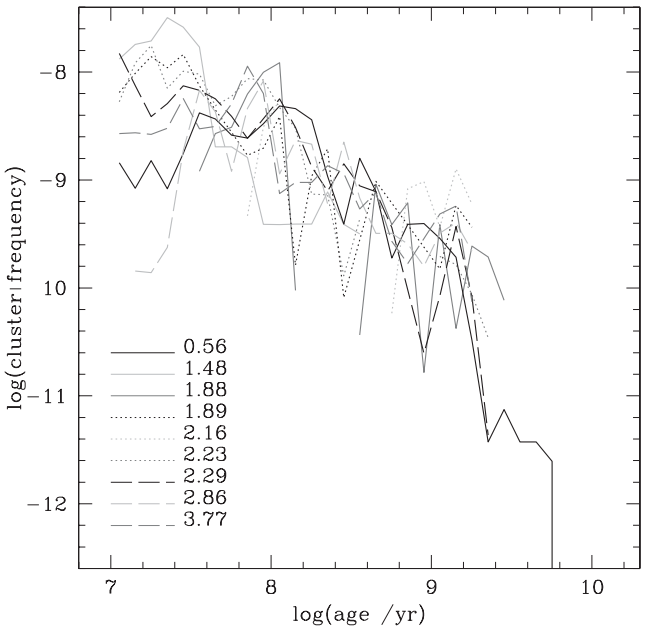

Figure 7. CFs for different LMC fields. The deprojected distances (°) of each field are indicated in the bottom-left corner.

7 CONCLUSIONS

The astrophysical properties of LMC star clusters have been the starting point to address galactic global issues such as the age–metallicity relationship and the cluster formation rate, among others. However, the number of clusters with estimated properties is by far less than a half of the catalogued clusters. Therefore, it is of great importance to enlarge the number of objects confirmed as genuine star clusters and to estimate their fundamental parameters.

We have used Washington photometry for 90 star cluster candidates of small angular size, typically ∼11 arcsec in radius, distributed within nine fields (36×36 arcmin^2) located in the LMC inner disc to estimate their ages and to build their local CFs. Some clusters are projected towards relatively crowded fields.

In order to assure a meaningful interpretation of the observed cluster CMDs, we applied a subtraction procedure to statistically clean them from the field star contamination. Thus, we could disentangle cluster features from those belonging to their surrounding fields. The employed technique makes use of variable cells in order to reproduce the field CMD as closely as possible.

Out of the 90 cluster candidates studied, 61 resulted to be genuine physical systems, whereas the remaining ones were classified as possible non-clusters since either their CMDs and/or the distribution of stars in the respective fields do not resemble those of stellar aggregates. We statistically show that $\sim(13 \pm 6)$ per cent of the catalogued clusters distributed within the inner disc (distance from the LMC $\leq 4°$) could be possible non-clusters, independently of their deprojected distances.

We derived the ages for the confirmed clusters from the fit of theoretical isochrones computed for the Washington system to the cleaned cluster CMDs. When adjusting a subset of isochrones, we took into account the LMC distance modulus and the individual star cluster colour excesses. The derived ages resulted to be in the age range $7.8 \leq \log(t) \leq 9.2$. Finally, we built CFs from ages available in the literature and from the ages estimated in this work, which encompass 90 per cent of the whole sample of catalogued clusters located in the studied LMC regions. We found that there exists some spatial variation of the LMC CF throughout the inner disc. Particularly, the innermost field (deprojected distance ∼0.°56) contains a handful of clusters older than ∼2 Gyr, while the wider spread between different CFs has taken place during the most recent 50 Myr of the galaxy lifetime.

ACKNOWLEDGEMENTS

We are grateful for the comments and suggestions raised by the anonymous referee which helped us to improve the manuscript. This research has made use of the SIMBAD data base, operated at CDS, Strasbourg, France, and draws upon data as distributed by the NOAO Science Archive. NOAO is operated by the Association of Universities for Research in Astronomy (AURA), Inc. under a cooperative agreement with the National Science Foundation. This work was partially supported by the Argentinian institutions CONICET and Agencia Nacional de Promoción Científica y Tecnológica (ANPCyT).

REFERENCES

Baumgardt H., Parmentier G., Anders P., Grebel E. K., 2013, MNRAS, 430, 676
Bica E., Geisler D., Dottori H., Clariá J. J., Piatti A. E., Santos J. F. C., Jr, 1998, AJ, 116, 723
Bica E., Bonatto C., Dutra C. M., Santos J. F. C., 2008, MNRAS, 389, 678 (B08)
Brocato E., Castellani V., Ferraro F. R., Piersimoni A. M., Testa V., 1996, MNRAS, 282, 614
Burstein D., Heiles C., 1982, AJ, 87, 1165 (BH)
Canterna R., 1976, AJ, 81, 228
Choudhury S., Subramaniam A., Piatti A., 2014, MNRAS, in press
de Grijs R., Goodwin S. P., Anders P., 2013, MNRAS, 436, 136
Geisler D., Sarajedini A., 1999, AJ, 117, 308
Geisler D., Bica E., Dottori H., Claria J. J., Piatti A. E., Santos J. F. C., Jr, 1997, AJ, 114, 1920
Geisler D., Piatti A. E., Bica E., Clariá J. J., 2003, MNRAS, 341, 771
Glatt K., Grebel E. K., Koch A., 2010, A&A, 517, A50 (G10)
Harris J., Zaritsky D., 2009, AJ, 138, 1243
Haschke R., Grebel E. K., Duffau S., 2011, AJ, 141, 158
Hunter D. A., Elmegreen B. G., Dupuy T. J., Mortonson M., 2003, AJ, 126, 1836
Mackey A. D., Gilmore G. F., 2003, MNRAS, 338, 85
Maia F. F. S., Piatti A. E., Santos J. F. C., 2014, MNRAS, 437, 2005
Marigo P., Girardi L., Bressan A., Groenewegen M. A. T., Silva L., Granato G. L., 2008, A&A, 482, 883
Olsen K. A. G., Salyk C., 2002, AJ, 124, 2045
Palma T., Clariá J. J., Geisler D., Piatti A. E., Ahumada A. V., 2013, A&A, 555, A131
Piatti A. E., 2011a, MNRAS, 416, L89
Piatti A. E., 2011b, MNRAS, 418, L40
Piatti A. E., 2011c, MNRAS, 418, L69
Piatti A. E., 2012a, MNRAS, 422, 1109
Piatti A. E., 2012b, A&A, 540, A58
Piatti A. E., 2014, MNRAS, 437, 1646 (P14)
Piatti A. E., Bica E., 2012, MNRAS, 425, 3085
Piatti A. E., Geisler D., 2013, AJ, 145, 17
Piatti A. E., Geisler D., Bica E., Clariá J. J., Santos J. F. C., Jr, Sarajedini A., Dottori H., 1999, AJ, 118, 2865
Piatti A. E., Sarajedini A., Geisler D., Bica E., Clariá J. J., 2002, MNRAS, 329, 556
Piatti A. E., Geisler D., Bica E., Clariá J. J., 2003a, MNRAS, 343, 851
Piatti A. E., Bica E., Geisler D., Clariá J. J., 2003b, MNRAS, 344, 965
Piatti A. E., Geisler D., Sarajedini A., Gallart C., 2009, A&A, 501, 585

Piatti A. E., Clariá J. J., Parisi M. C., Ahumada A. V., 2011, PASP, 123, 519
Piatti A. E., Geisler D., Mateluna R., 2012, AJ, 144, 100
Pietrzyński G., Udalski A., 2000, Acta Astron., 50, 337
Pietrzyński G. et al., 2013, Nature, 495, 76
Popescu B., Hanson M. M., Elmegreen B. G., 2012, ApJ, 751, 122 (P12)
Schlegel D. J., Finkbeiner D. P., Davis M., 1998, ApJ, 500, 525
Subramanian S., Subramaniam A., 2009, A&A, 496, 399
Subramanian S., Subramaniam A., 2010, A&A, 520, A24
Udalski A., 2003, Acta Astron., 53, 291
Zaritsky D., Harris J., Thompson I. B., Grebel E. K., Massey P., 2002, AJ, 123, 855

SUPPORTING INFORMATION

Additional Supporting Information may be found in the online version of this article:

Figure. 90 multi-panel figures like Fig. 2 (http://mnras.oxfordjournals.org/lookup/suppl/doi:10.1093/mnras/stu534/-/DC1).

Please note: Oxford University Press is not responsible for the content or functionality of any supporting materials supplied by the authors. Any queries (other than missing material) should be directed to the corresponding author for the paper.

This paper has been typeset from a TEX/LATEX file prepared by the author.